THE NEW ANALYTICAL STUDY FOR BOUNDARY-LAYER SLIP FLOW AND HEAT TRANSFER OF NANOFLUID OVER A STRETCHING SHEET

by

Fazle MABOOD[a], Waqar A. KHAN[b], and Muhammad Mehdi RASHIDI[c,d,e*]

[a] Department of Mathematics, Edwardes College Peshawar, Peshawar, Pakistan
[b] Department of Mechanical Engineering, University of Waterloo, Waterloo, Ont., Canada
[c] Shanghai Key Laboratory of Vehicle Aerodynamics and Vehicle Thermal Management Systems, Shanghai, China
[d] ENN-Tongji Clean Energy Institute, Shanghai, China
[e] Department of Civil Engineering, School of Engineering, University of Birmingham, Birmingham, UK

Original scientific paper
DOI:10.2298/TSCI140424035M

In this article, the semi-analytical numerical technique known as the homotopy analysis method is employed to derive solutions for partial slip effects on the heat transfer of nanofluids over a stretching sheet. An accurate analytical solution is presented which depends on the Prandtl number, slip factor, Lewis number, Brownian motion number, and thermophoresis number. The variation of the reduced Nusselt and reduced Sherwood numbers with Brownian motion number, and thermophoresis number for various values Prandtl number, slip factor, Lewis number is presented in tabular and graphical forms. The results of the present article show the flow velocity and the surface shear stress on the stretching sheet and also reduced Nusselt number and Sherwood number are strongly influenced by the slip parameter. It is found that hydrodynamic boundary-layer decreases and thermal boundary-layer increases with slip parameter. Comparison of the present analysis is made with the previously existing literature and an appreciable agreement in the values is observed for the limiting case.

Key words: *nanofluid, velocity slip, stretching sheet, auxiliary parameter, homotopy analysis method solution*

Introduction

The enhancement in thermal conductivity of conventional fluids through suspensions of solid particles is a recent development in engineering technology aimed at increasing the coefficient of heat transfer. The thermal conductivity of solid metals is higher than the base fluids, so the suspended particles are able to increase the thermal conductivity and heat transfer performance. Choi and Eastman [1] were most likely the first researchers to combine a mixture of nanoparticles and base fluid, which they subsequently termed a *nanofluid*, and it was adopted by many researchers. The materials with sizes of nanometers possess sole physical and chemical properties. They can flow smoothly through micro-channels without clogging them because they are small enough to behave similarly to liquid molecules [2].

* Corresponding author, e-mail: mm_rashidi@sjtu.edu.cn; mm_rashidi@yahoo.com

Nanofluids offer many diverse advantages in industrial application such as microelectronics, fuel cell, nuclear reactors, biomedicine, and transportation, many of which have been reviewed by Wong and Leon [3]. Hwang *et al.* [4] measured the thermal conductivities of various nanofluids and verified that the volume fraction of suspended particle is the effective parameter in enhancing the thermal conductivity. Several numerical studies related to regular fluid/nanofluids have been reported in the literature [5-16].

Recently, the Cheng-Minkowycz model for natural convective boundary-layer flow in a porous medium saturated by a nanofluid is investigated by Nield and Kuznetsov [17]. For natural convective boundary-layer nanofluid flow over a vertical surface is reported by Kuznetsov and Nield [18]. Khan and Pop [19] numerically studied the laminar nanofluid transport phenomena from a stretching sheet. Bachok *et al.* [20] have analyzed steady boundary-layer nanofluid flow over a moving semi-infinite flat plate. Rana and Bhargava [21] used finite element and finite difference methods to study nanofluid heat and mass transfer from a non-linearly stretching sheet. Buongiorno [22] investigated the steady buoyancy-driven dissipative magnetoconvective flow from a vertical non-linear stretching sheet. Abel *et al.* [23] have produced the exact solutions at various values of the physical parameters for the model studied by Khan and Pop [19]. In all previous studies, the researchers ignored the slip effects at the wall.

Majumder *et al.* [24] have shown that the nanofluidic flow generally exhibits partial slip against the solid surface, which can be characterized by slip-length (around 3.4-68 mm for different liquids). Wang [25] reported that the partial slip between the fluid and the moving stretching surface, Sahoo and Do [26] examined the slip effects on third grade fluid over stretching sheet. Noghrehabadi *et al*. [27] investigated the effect of partial slip boundary condition on nanofluid flow and heat transfer over a stretching sheet at constant wall temperature, while Aly *et al.* [28] utilized Chebyshev pseudo-spectral differentiation matrix to obtain the exact solution for the nanofluid flow model. Rashidi *et al* [29] and Rashidi and Erfani [30] investigated slip condition of MHD flow in different physical situations. Taking into account the significance of the partial slip previously mentioned, in the present work we derive semi-analytical solutions for boundary-layer flow and heat transfer of nanofluid over stretching sheet with constant wall temperature using homotopy analysis method (HAM) which was proposed by Liao [31]. Numerous researchers have successfully applied HAM on many physical problems in science and engineering [32-41].

The considered problem studied first by Noghrehabadi *et al*. [27] and exerted the similarity solution.

Flow analysis and mathematical formulation

Consider a 2-D, steady and incompressible viscous flow of a nanofluid past over a stretching surface. The velocity of the surface is considered to be linear, *i. e* $U_w(x) = cx$. Here, c is constant and x is co-ordinate measured along the surface. The nanofluid flows at $y = 0$, where y is the co-ordinate normal to the surface. We assumed that the wall temperature, T_w, and the nanoparticle fraction, φ_w, are constant at stretching surface. When y tends to infinity, the ambient values of temperature and nanoparticle fraction are denoted by T_∞ and φ_∞, respectively. The co-ordinate system and the flow model are shown in fig. 1. For nanofluids, in Cartesian co-ordinates system of x and y, the governing steady conservation of momentum, thermal energy, and nanoparticles equations including the dynamic effects of nanoparticles can be written [19]:

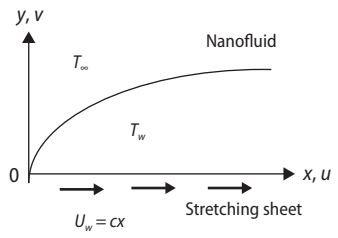

Figure 1. Schematic diagram of the problem

$$\frac{\partial u}{\partial x}+\frac{\partial v}{\partial y}=0 \tag{1}$$

$$u\frac{\partial u}{\partial x}+v\frac{\partial u}{\partial y}=-\frac{1}{\rho_{\mathrm{f}}}\frac{\partial p}{\partial x}+\nu\left(\frac{\partial^2 u}{\partial x^2}+\frac{\partial^2 u}{\partial y^2}\right) \tag{2}$$

$$u\frac{\partial v}{\partial x}+v\frac{\partial v}{\partial y}=-\frac{1}{\rho_{\mathrm{f}}}\frac{\partial p}{\partial y}+\nu\left(\frac{\partial^2 v}{\partial x^2}+\frac{\partial^2 v}{\partial y^2}\right) \tag{3}$$

$$u\frac{\partial T}{\partial x}+v\frac{\partial T}{\partial y}=\alpha\left(\frac{\partial^2 T}{\partial x^2}+\frac{\partial^2 T}{\partial y^2}\right)+\tau\left\{D_B\left(\frac{\partial\varphi}{\partial x}\frac{\partial T}{\partial x}+\frac{\partial\varphi}{\partial y}\frac{\partial T}{\partial y}\right)+\frac{D_T}{T_\infty}\left[\left(\frac{\partial T}{\partial x}\right)^2+\left(\frac{\partial T}{\partial y}\right)^2\right]\right\} \tag{4}$$

$$u\frac{\partial\varphi}{\partial x}+v\frac{\partial\varphi}{\partial y}=D_B\left(\frac{\partial^2\varphi}{\partial x^2}+\frac{\partial^2\varphi}{\partial y^2}\right)+\left(\frac{D_B}{T_\infty}\right)\left(\frac{\partial^2 T}{\partial x^2}+\frac{\partial^2 T}{\partial y^2}\right) \tag{5}$$

The boundary conditions for the velocity components, temperature, and nanoparticle fraction are defined:

$$u=U_w-U_s,\quad v=0,\quad T=T_w,\quad \varphi=\varphi_w\quad \text{for}\quad y=0 \tag{6}$$

$$u=0,\quad v=0,\quad T=T_\infty,\quad \varphi=\varphi_\infty\quad \text{for}\quad y=\infty \tag{7}$$

Here, u and v are the velocity components along the axis x and y, respectively, p – the fluid pressure, α – the thermal diffusivity, ν – the kinematic viscosity, ρ_f – the density of the base fluid, U_s – the velocity slip at the wall, D_B – the Brownian diffusion coefficient, and D_T – the thermophoresis diffusion coefficient. The $\tau=(\rho c)_{\mathrm{p}}/(\rho c)_{\mathrm{f}}$ is the ratio between the effective heat capacity of the nanoparticle material and heat capacity of the fluid with ρ being the density, c – the volumetric volume coefficient, ρ_{p} – the density of the particles, and φ – rescaled nanoparticle volume fraction.

Noghrehabadi *et al*. [27] introduced the following transformations:

$$\psi=\sqrt{c\nu}\,xf(\eta),\quad \eta=y\sqrt{\frac{c}{\nu}},\quad \theta(\eta)=\frac{T-T_\infty}{T_w-T_\infty},\quad \phi(\eta)=\frac{\varphi-\varphi_\infty}{\varphi_w-\varphi_\infty} \tag{8}$$

where ψ represent the stream function and is defined as $u=\partial\psi/\partial y$, $v=-\partial\psi/\partial x$, so that eq. (1) satisfied identically. We have taken into account that the pressure in the outer (inviscid) flow is $p=p_0$ (constant). Hence, the flow occurs only due to the stretching of the sheet, therefore, the pressure gradient can be neglected. The governing equations are reduced by using eq. (8) as:

$$f'''+ff''-f'^2=0 \tag{9}$$

$$\frac{1}{\mathrm{Pr}}\theta''+f\theta'+Nb\phi'\theta'+Nt\theta'^2=0 \tag{10}$$

$$\phi''+\frac{Nt}{Nb}\theta''+\mathrm{Le}\,f\phi'=0 \tag{11}$$

Here, by using boundary-layer approximations and introducing Navier's condition the velocity on the surface can be written:

$$u - U_w = N\rho\nu\frac{\partial u}{\partial y} = U_s \tag{12}$$

where ρ is the density and N is the slip constant. Using similarity transformations eq. (12) reduces to:

$$f'(0) - 1 = \lambda f''(0) \tag{13}$$

where $\lambda = N\rho\sqrt{c\nu}$ is the dimensionless slip factor. Equations (9)-(11) can solved analytically subject to the transformed boundary conditions:

$$\begin{aligned} &f(0) = 0,\ \ f'(0) = 1 + \lambda f''(0),\ \ f'(\infty) = 0, \\ &\theta(0) = 1,\ \ \theta(\infty) = 0,\ \ \phi(0) = 1,\ \ \phi(\infty) = 0 \end{aligned} \tag{14}$$

where primes denote differentiation with respect to η and the four parameters are defined:

$$\mathrm{Pr} = \frac{\nu}{\alpha},\quad \mathrm{Le} = \frac{\nu}{D_B},\quad Nb = \frac{(\rho c)_\mathrm{p} D_B(\phi_w - \phi_\infty)}{(\rho c)_\mathrm{f}\nu},\quad Nt = \frac{(\rho c)_\mathrm{p} D_T(T_w - T_\infty)}{(\rho c)_\mathrm{f} T_\infty \nu} \tag{15}$$

Here, Pr, Le, *Nb* and *Nt* denote the Prandtl number, Lewis number, Brownian motion parameter, and thermophoresis parameter, respectively. It is important to note that this boundary value problem reduces to the classical problem of flow and heat and mass transfer due to a stretching surface in a viscous fluid when *Nb* and *Nt* are zero in eqs. (10) and (11). (The boundary value problem for ϕ then becomes ill-posed and is of no physical significance).

In the continuum modeling of fluidic transport, nanofluid usually exhibits partial slip against the solid surface, which can be characterized by the so-called slip length (around 3.4 to 68 mm for different liquids). Most nanofluids examined to date have large values for the Lewis number, Le > 1 [24]. For water nanofluids at room temperature with nanoparticles of 1 to 100 nm diameters, the Brownian diffusion coefficient, D_B, ranges from $4\cdot10^{-4}$ to $4\cdot10^{-12}$ m^2/s [24]. Furthermore, the ratio of Brownian diffusivity coefficient to thermophoresis coefficient for particles with diameters of 1 to 100 nm can be varied in the ranges of 2 to 0.02 for Al, and from 2 to 20 for Cu nanoparticles. Rana and Bhargava [21] studied *Nb* and *Nt* in the range of 0.1 to 0.5 and Lewis number in the range of 1 to 25 for the nanofluid boundary-layer over the stretching sheets. Hence, the variation of dimensionless parameters of nanofluids in the present study is considered to vary in the mentioned range.

The quantities of practical interest, in this study, are the Nusselt number and the Sherwood number which are defined:

$$\mathrm{Nu} = \frac{-xq_w}{k(T_w - T_\infty)},\quad \mathrm{Sh} = \frac{xq_m}{D_B(\varphi_w - \varphi_\infty)} \tag{16}$$

where q_w and q_m are the wall heat and mass fluxes, respectively. Using eq. (8), we obtain:

$$\mathrm{Re}_x^{-1/2}\,\mathrm{Nu} = -\theta'(0),\quad \mathrm{Re}_x^{-1/2}\,\mathrm{Sh} = -\phi'(0) \tag{17}$$

where $\mathrm{Re}_x = U_w(x)/\nu$ is the local Reynolds number based on the stretching velocity $U_w(x)$. It is interesting to note that Wang [25] obtained an exact solution for eq. (9) subject to the boundary conditions (14).

The HAM solution

The dimensionless velocity $f'(\eta)$, temperature $\theta(\eta)$, and concentration $\phi(\eta)$ profiles can be expressed by the set of base functions:

$$\left\{\eta^k \exp(-n\eta)\middle| k \geq 0, n \geq 0\right\} \tag{18}$$

in the form of following series:

$$\begin{aligned} f(\eta) &= \sum_{n=0}^{\infty}\sum_{k=0}^{\infty} a_{m,n}^{k}\eta^k \exp(-n\eta), \\ \theta(\eta) &= \sum_{n=0}^{\infty}\sum_{k=0}^{\infty} b_{m,n}^{k}\eta^k \exp(-n\eta), \\ \phi(\eta) &= \sum_{n=0}^{\infty}\sum_{k=0}^{\infty} c_{m,n}^{k}\eta^k \exp(-n\eta) \end{aligned} \tag{19}$$

where $a_{m,n}^{k}$, $b_{m,n}^{k}$, and $c_{m,n}^{k}$ are the coefficients. We choose the initial guesses $f_0(\eta)$, $\theta_0(\eta)$, and $\phi_0(\eta)$ based on boundary condition (14) and the Liao [31] *rule of solution expression*:

$$f_0(\eta) = \frac{1}{1+\lambda}\left(1-\mathrm{e}^{-\eta}\right), \quad \theta_0(\eta) = \mathrm{e}^{-\eta}, \quad \phi_0(\eta) = \mathrm{e}^{-\eta} \tag{20}$$

The linear operators L_1, L_2, and L_3 in the following way:

$$L_1(f) = \frac{\mathrm{d}^3 f}{\mathrm{d}\eta^3} + \frac{\mathrm{d}^2 f}{\mathrm{d}\eta^2}, \quad L_2(\theta) = \frac{\mathrm{d}^2\theta}{\mathrm{d}\eta^2} + \frac{\mathrm{d}\theta}{\mathrm{d}\eta}, \quad L_3(\phi) = \frac{\mathrm{d}^2\phi}{\mathrm{d}\eta^2} + \frac{\mathrm{d}\phi}{\mathrm{d}\eta} \tag{21}$$

The operators L_1, L_2, and L_3 have the following properties:

$$L_1(C_1 + C_2\eta + C_3\mathrm{e}^{-\eta}) = 0, \quad L_2(C_4 + C_5\mathrm{e}^{-\eta}) = 0, \quad L_3(C_6 + C_7\mathrm{e}^{-\eta}) = 0 \tag{22}$$

where C_i (i = 1-5) are arbitrary constants. Let $q \in [0,1]$ represents an embedding parameter and $\hbar \neq 0$ be the auxiliary parameter to adjust the convergence rate of the perturbation series. We construct the following 0th order deformation of the problem:

$$(1-q)L_1\left[\hat{f}(\eta;q) - f_0(\eta)\right] = q\hbar_f N_1\left[\hat{f}(\eta;q)\right] \tag{23}$$

$$(1-q)L_2\left[\hat{\theta}(\eta;q) - \theta_0(\eta)\right] = q\hbar_\theta N_2\left[\hat{f}(\eta;q), \hat{\theta}(\eta;q)\right] \tag{24}$$

$$(1-q)L_3\left[\hat{\phi}(\eta;q) - \phi_0(\eta)\right] = q\hbar_\phi N_3\left[\hat{f}(\eta;q), \hat{\phi}(\eta;q)\right] \tag{25}$$

subject to the conditions:

$$\hat{f}(0;q) = 0, \quad \hat{f}'(0;q) = 1 + \lambda\hat{f}''(0;q), \quad \hat{f}'(\infty;q) = 0 \tag{26}$$

$$\hat{\theta}(0;q) = 1, \quad \hat{\theta}(\infty;q) = 0, \quad \hat{\phi}(0;q) = 1, \quad \hat{\phi}(\infty;q) = 0 \tag{27}$$

where the non-linear operators are defined:

$$N_1 = \frac{\partial^3 \hat{f}(\eta;q)}{\partial \eta^3} + \hat{f}(\eta;q)\frac{\partial^2 \hat{f}(\eta;q)}{\partial \eta^2} - \left[\frac{\partial \hat{f}(\eta;q)}{\partial \eta}\right]^2 \tag{28}$$

$$N_2 = \frac{1}{\mathrm{Pr}}\frac{\partial^2 \hat{\theta}(\eta;q)}{\partial \eta^2} + \hat{f}(\eta;q)\frac{\partial \hat{\theta}(\eta;q)}{\partial \eta} + Nb\frac{\partial \hat{\phi}(\eta;q)}{\partial \eta}\frac{\partial \hat{\theta}(\eta;q)}{\partial \eta} + Nt\frac{\partial^2 \hat{\theta}(\eta;q)}{\partial \eta^2} \tag{29}$$

$$N_3 = \frac{\partial^2 \hat{\phi}(\eta;q)}{\partial \eta^2} + \frac{Nt}{Nb}\frac{\partial^2 \hat{\theta}(\eta;q)}{\partial \eta^2} + \mathrm{Le}\,\hat{f}(\eta;q)\frac{\partial \hat{\phi}(\eta;q)}{\partial \eta} \tag{30}$$

For $q = 0$ and $q = 1$ we have:

$$\hat{f}(q;\eta;0) = f_0(q;\eta), \qquad \hat{f}(q;\eta;1) = f(q;\eta) \tag{31}$$

$$\hat{\theta}(q;\eta;0) = \theta_0(q;\eta), \qquad \hat{\theta}(q;\eta;1) = \theta(q;\eta) \tag{32}$$

$$\hat{\phi}(q;\eta;0) = \phi_0(q;\eta), \qquad \hat{\phi}(q;\eta;1) = \phi(q;\eta) \tag{33}$$

Defining:

$$f_m(\eta) = \frac{1}{m!}\frac{\partial^m f(\eta;q)}{\partial q^m}\bigg|_{q=0}, \quad \theta_m(\eta) = \frac{1}{m!}\frac{\partial^m \theta(\eta;q)}{\partial q^m}\bigg|_{q=0}, \quad \phi_m(\eta) = \frac{1}{m!}\frac{\partial^m \phi(\eta;q)}{\partial q^m}\bigg|_{q=0} \tag{34}$$

and expanding $\hat{f}(q;\eta)$, $\hat{\theta}(q;\eta)$, and $\hat{\phi}(q;\eta)$ by means of Taylor's theorem with respect to q, we obtain:

$$\hat{f}(q;\eta) = f_0(\eta) + \sum_{m=1}^{\infty} f_m(\eta) q^m \tag{35}$$

$$\hat{\theta}(q;\eta) = \theta_0(\eta) + \sum_{m=1}^{\infty} \theta_m(\eta) q^m \tag{36}$$

$$\hat{\phi}(q;\eta) = \phi_0(\eta) + \sum_{m=1}^{\infty} \phi_m(\eta) q^m \tag{37}$$

The auxiliary parameters are properly chosen so that series eqs. (35)-(37) converge at $q = 1$ and thus:

$$f(\eta) = f_0(\eta) + \sum_{m=1}^{\infty} f_m(\eta) \tag{38}$$

$$\theta(\eta) = \theta_0(\eta) + \sum_{m=1}^{\infty} \theta_m(\eta) \tag{39}$$

$$\phi(\eta) = \phi_0(\eta) + \sum_{m=1}^{\infty} \phi_m(\eta) \tag{40}$$

The resulting problems at the mth order deformation are:

$$L_1\left[f_m(\eta)-\chi_m f_{m-1}(\eta)\right]=\hbar_f \mathrm{R}_m^f(\eta) \tag{41}$$

$$L_2\left[\theta_m(\eta)-\chi_m \theta_{m-1}(\eta)\right]=\hbar_\theta \mathrm{R}_m^\theta(\eta) \tag{42}$$

$$L_3\left[\phi_m(\eta)-\chi_m \phi_{m-1}(\eta)\right]=\hbar_\phi \mathrm{R}_m^\phi(\eta) \tag{43}$$

$$f_m(0)=0,\ f_m'(0)=\lambda f_m''(0),\ f_m'(\infty)=0,\ \theta_m(0)=0,\ \theta_m(\infty)=0,\phi_m(0)=0,\ \phi_m(\infty)=0 \tag{44}$$

$$\mathrm{R}_m^f(\eta)=f_{m-1}'''+\sum_{k=0}^{m-1}\left(f_k f_{m-1-k}''-f_k' f_{m-1-k}'\right) \tag{45}$$

$$\mathrm{R}_m^\theta(\eta)=\frac{1}{\mathrm{Pr}}\theta_{m-1}''+\sum_{k=0}^{m-1}f_k\theta_{m-1-k}'+Nb\sum_{k=0}^{m-1}\phi_k'\theta_{m-1-k}'+Nt\sum_{k=0}^{m-1}\theta_k'\theta_{m-1-k}' \tag{46}$$

$$\mathrm{R}_m^\phi(\eta)=\phi_{m-1}''+\left(\frac{Nt}{Nb}\right)\theta_{m-1}''+\mathrm{Le}\sum_{k=0}^{m-1}f_k\phi_{m-1-k}' \tag{47}$$

$$\chi_m=\begin{cases}0, & m\le 1,\\ 1, & m>1\end{cases} \tag{48}$$

The general solutions of eqs. (41)-(43) can be written:

$$f_m(\eta)=f_m^*(\eta)+C_1+C_2\eta+C_3\mathrm{e}^{-\eta} \tag{49}$$

$$\theta_m(\eta)=\theta_m^*(\eta)+C_4+C_5\mathrm{e}^{-\eta} \tag{50}$$

$$\phi_m(\eta)=\phi_m^*(\eta)+C_6+C_7\mathrm{e}^{-\eta} \tag{51}$$

where $f_m^*(\eta)$, $\theta_m^*(\eta)$, and $\phi_m^*(\eta)$ are the particular solutions and the constants and should be determined by the boundary condition eq. (44).

Convergence of homotopy solution

Liao [31] has mentioned that the convergence rate of approximation of the HAM solution is strongly dependent upon the values of non-zero auxiliary parameter $\hbar$. As the eqs. (49)-(51) involve $\hbar_f$, $\hbar_\theta$, and $\hbar_\phi$, so we can adjust the convergence of our HAM solution. To compute the range of admissible values of $\hbar_f$, $\hbar_\theta$, and $\hbar_\phi$, we display the $\hbar$-curves of the function $f''(0)$, $\theta'(0)$, and $\phi'(0)$ for 14th orders of approximations. Figure 2 depicts that range for the admissible values of $\hbar$-curves are $-0.85\le\hbar_f\le-0.3$, $-0.75\le\hbar_\theta\le-0.25$, and $-0.7\le\hbar_\phi\le-0.2$. Figure 2 shows the $\hbar$-curves for the dimensionless velocity, temperature, and concentration profiles. Convergence of the series solution up to 40th order of approx-

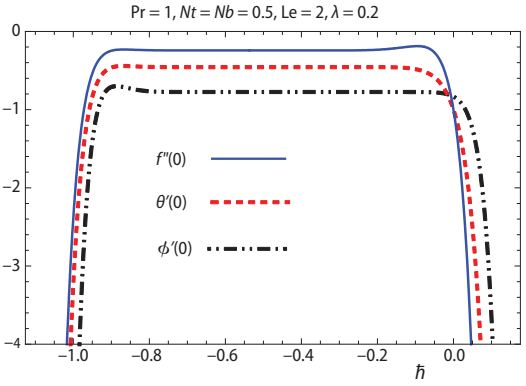

Figure 2. Combined $\hbar$-curves for $f''(0)$, $\theta'(0)$, and $\phi'(0)$ at 14th order of approximations

Table 1. Convergence of HAM solution for different order of approximations at Pr = 1, $Nt = Nb = 0.5$, Le = 2, $\lambda = 0{,}2$, and $\hbar_f = \hbar_\theta = \hbar_\phi = -0.5$

Order of approximations	$f''(0)$	$-\theta'(0)$	$-\phi'(0)$
1	–0.76389	0.45833	0.41667
5	–0.77460	0.31144	0.71088
10	–0.77470	0.32200	0.70212
15	–0.77470	0.32222	0.69995
21	–0.77470	0.32217	0.70004
25	–0.77470	0.32217	0.70004
30	–0.77470	0.32217	0.70004
40	–0.77470	0.32217	0.70004

imations is presented in tab. 1. It is found from tab. 1 that the convergence is achieved up to 21st order of approximation.

Results and discussions

The non-linear ordinary differential eqs. (9)-(11) together with boundary condition (14) are solved analytically using HAM. The HAM computations have been carried out for various range of slip boundary condition and for different values of parameters such as Prandtl number, the Lewis number, the Brownian motion parameter, and the thermophoresis parameter. The effects of the emerging parameters on dimensionless velocity, temperature, the rate of heat and mass transfer, and the nanoparticle volume fraction are investigated and presented graphically in figs. 3-10. As a test of accuracy of the HAM solution, comparison has been done between the results of HAM and previously published study [15, 22-24] for $-f''(0)$, $-\theta'(0)$, and $-\phi'(0)$ in tabs. 2-4 which confirm that the present simulation is accurate.

Figure 3 exhibits the effect of slip parameter on the velocity and shear stress. An examination of fig. 3 reveals that with the increase in velocity slip parameter, λ, the fluid velocity decreases because in the case of slip condition, the effect of the pull of the stretching sheet is

Table 2. Comparison of $-f''(0)$ for several values of slip factor

λ	[25]	[26]	[27]	HAM solution
0.0	1.0	1.001154	1.0	1.0
0.1	–	0.871447	0.872082	0.872082
0.3	0.701	0.699738	0.701548	0.701548
0.5	–	0.589195	0.591195	0.591195
1	0.430	0.428450	0.430160	0.430160
2	0.284	0.282893	0.283980	0.283981
5	0.145	0.144430	0.144841	0.144843
10	–	0.081091	0.081243	0.081246

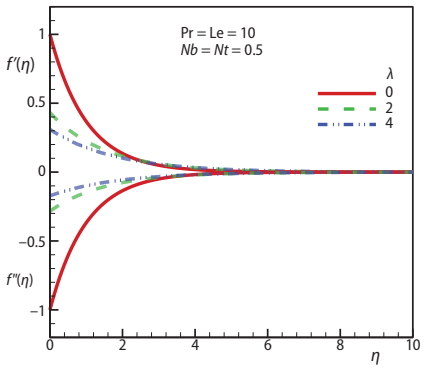

Figure 3. Effects of slip factor on dimensionless velocity

Table 3. Comparison of the results of $-\theta'(0)$ and $-\phi'(0)$ when Pr = Le = 10 and $\lambda = 0$

Nb	Nt	$-\theta'(0)$			$-\phi'(0)$		
		[19]	[27]	HAM	[19]	[27]	HAM
0.1	0.1	0.9524	0.9523768	0.9523767	2.1294	2.1293938	2.1293938
	0.2	0.6932	0.6931743	0.6931743	2.2740	2.2740215	2.2740215
	0.3	0.5201	0.5200790	0.5200790	2.5286	2.5286382	2.5286381
	0.4	0.4026	0.4025808	0.4025810	2.7952	2.7951701	2.7951703
	0.5	0.3211	0.3210543	0.3210544	3.0351	3.0351425	3.0351425
0.2		0.5056	0.5055814	0.5055814	2.3819	2.3818706	2.3818707
0.3		0.2522	0.2521560	0.2521560	2.4100	2.4100188	2.4100188
0.4		0.1194	0.1194059	0.1194059	2.3997	2.3996502	2.3996502
0.5		0.0543	0.0542534	0.0542534	2.3836	2.3835712	2.3835712

Table 4. Comparison of the results of $-\theta'(0)$ and $-\phi'(0)$ when Pr = Le = 10

λ	Nt	Nb	$-\theta'(0)$		$-\phi'(0)$	
			[27]	HAM	[27]	HAM
0.5	0.2	0.1	0.424328	0.424328	1.99907	1.999072
		0.2	0.306640	0.306640	2.11099	2.110993
		0.3	0.229206	0.229207	2.228691	2.228691
1	0.3	0.1	0.190347	0.190346	1.819268	1.819267
		0.2	0.137084	0.137084	1.898513	1.898513
		0.3	0.102297	0.102297	1.969337	1.969337

only partially transmitted to the fluid as shown in fig. 3. It is further observe that maximum velocity occur for $\lambda = 0$. The velocity curves show that the rate of transport decreases with the increasing distance, η, normal to the sheet. In addition, it is noticed that the magnitude of shear stress decreases with the slip parameter.

Figures 4 and 5 illustrate the dimensionless temperature and concentration profiles for various values of the slip parameter. The temperature and nanoparticle concentration are clearly observed to be significantly enhanced with increasing slip parameter values. Figure 6 exhibits

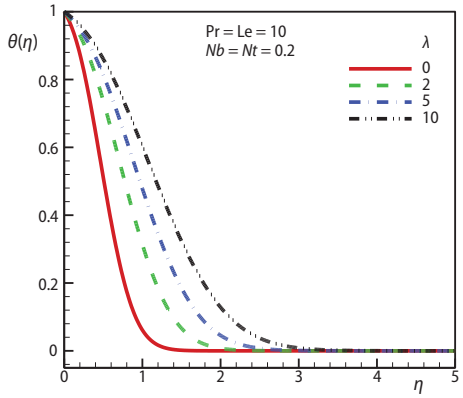

Figure 4. Effects of slip factor on dimensionless temperature

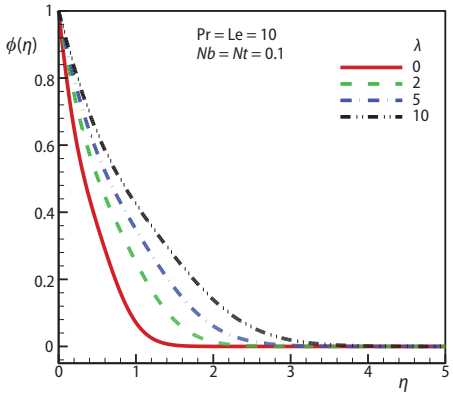

Figure 5. Effects of slip factor on dimensionless concentration

the effect of the Prandtl number on the dimensionless temperature. It is observed that the thermal boundary-layer significantly decrease with Prandtl number. This is because the decrease in Prandtl number leads to the increase in the thermal conductivity of the fluid so that heat is able to diffuse away from the heated surface more quickly. Hence, for the smaller values of Prandtl number the thermal boundary-layer is thicker. Figure 7 shows the effect of the Lewis number on the concentration profile for selected parameters. The concentration boundary-layer thickness reduces when the Lewis number values intensify.

The variation of the Nusselt number with slip boundary condition, the thermophoresis parameter

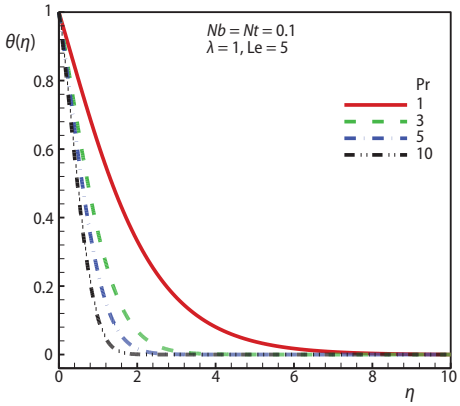

Figure 6. Effects of Prandtl number on dimensionless temperature

and Prandtl number is presented in fig. 8. It is observed that the dimensionless heat transfer rate is higher for variation of slip factor, λ, in smaller values of the thermophoresis parameter, Nt, and this change decreases with the increase of Nt. It is also seen that in the absence of slip parameter the heat transfer rate is maximum. In addition, it is noticed that the Nusselt number increase with the Prandtl number because higher Prandtl number corresponds to thinner thermal boundary-layer. In figs. 9 and 10 the variation of reduced Sherwood number with slip boundary condition, Prandtl number, the thermophoresis parameter, and Lewis number is observed. It is noticed from fig. 9 that the dimensionless mass transfer rates with increase in thermophoresis parameter is decreased for small Prandtl numbers and increased for larger values of Prandtl number. In both situations, increase in slip factor results in decrease in Sherwood number. It is observed from fig. 10 that the increase of Lewis number increases the dimensionless mass transfer rates.

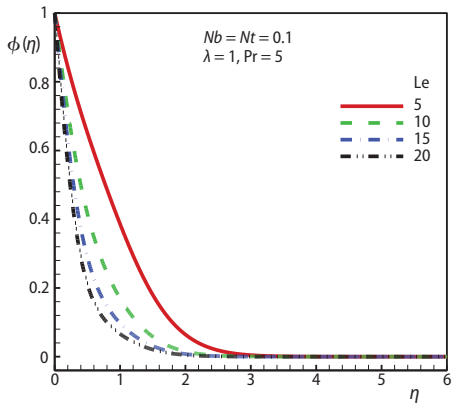

Figure 7. Effects of Lewis number on dimensionless concentration

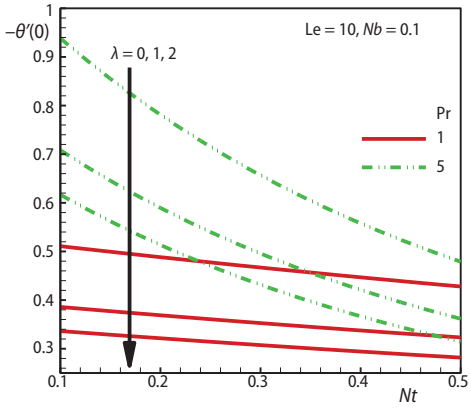

Figure 8. Variations of dimensionless heat transfer rates with slip factor, thermophoresis parameter, and Prandtl number

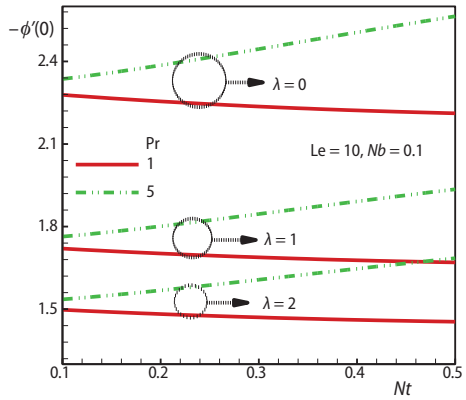

Figure 9. Variations of dimensionless concentration rates with slip factor, thermophoresis parameter, and Prandtl number

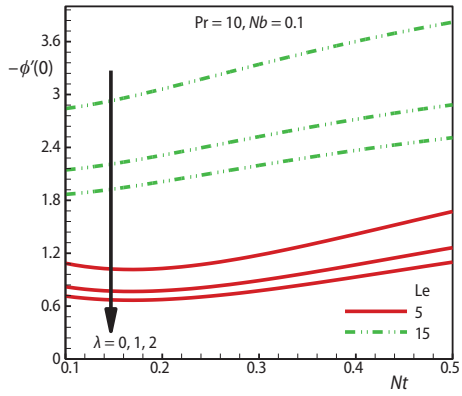

Figure 10. Variations of dimensionless concentration rates with slip factor and Lewis number

Conclusions

In this paper, HAM is applied to obtain the approximate solutions of heat transfer of a nanofluid fluid past a stretching sheet with slip boundary condition. The validity of our

solutions is verified by the numerical published data. The analytical solution presented which depends on the slip parameter, Prandtl number, Brownian motion number, Lewis number, and thermophoresis number. The variation of reduced Nusselt and Sherwood numbers with *Nt* and λ for various values of Prandtl and Lewis number is presented in both tabular and graphical forms. The main observations of the present study are as follows:

- Slip parameter decrease the momentum boundary-layer thickness while the temperature and concentration are increased.
- The reduced Nusselt and Sherwood numbers are the decreasing functions of slip parameter.
- Increasing Prandtl number increase the reduced Sherwood number.
- The reduced Nusselt number is the decreasing function of *Nt* and *Nb*.
- The reduced Sherwood number is the increasing function of *Nt* and Lewis number.

Nomenclature

c – volumetric volume coefficient
D_B – Brownian diffusion coefficient
D_T – thermophoresis diffusion coefficient
f – similarity function for velocity
k – thermal conductivity, [$Wm^{-1}K^{-1}$]
Le – Lewis number
Nb – Brownian motion parameter
Nt – thermophoresis parameter
N – slip constant
Nu – local Nusselt number
Pr – Prandtl number
p – constant presure
q_m – wall mass flux, [Wm^{-2}]
q_w – wall heat flux, [Wm^{-2}]
Re_x – local Reynolds number
Sh – Sherwood number
T – temperature, [K]
T_w – surface temperature, [K]
T_∞ – ambient temperature, [K]
U_s – velocity slip, [ms^{-1}]
U_w – stretching velocity, [ms^{-1}]
u – velocity in x-direction, [ms^{-1}]
v – velocity in y-direction, [ms^{-1}]
x – co-ordinate along the plate, [m]
y – co-ordinate normal to the sheet, [m]

Greek symbols

α – thermal diffusivity, [m^2s^{-1}]
η – similarity independent variable
θ – similarity function for temperature
λ – slip parameter
ν – kinematic viscosity, [$kgm^{-1}s^{-1}$]
ρ – fluid density, [kgm^{-3}]
ρ_f – density of the base fluid, [kgm^{-3}]
ρ_p – density of the particles, [kgm^{-3}]
ϕ_m – nanoparticle volume fraction
ψ – stream function

References

[1] Choi, S. U. S., Eastman, J. A., Enhancing Thermal Conductivity of Fluids with Nanoparticles, *Mater. Sci., 231* (1995), Nov., pp. 99-105
[2] Khanafer, K., *et al.,* Buoyancy Driven Heat Transfer Enhancement in a Two-Dimensional Enclosure Utilizing Nanofluids, *Int. J. Heat Mass Transf., 46* (2013), 19, pp. 3639-3653
[3] Wong, K. V., Leon, O. D., Applications of Nanofluids: Current and Future, *Adv. Mech. Eng., 2010* (2010), Nov., pp. 1-12
[4] Hwang, K. S., *et al.,* Buoyancy Driven Heat Transfer of Water-Based Al_2O_3 Nanofluids in a Rectangular Cavity, *Int. J. Heat Mass Transf., 50* (2007), 19-20, pp. 4003-4010
[5] Mansur, S., Ishak, A., The Flow and Heat Transfer of a Nanofluid past a Stretching/Shrinking Sheet with a Convective Boundary Condition, *Abst. Appl. Analy., 2013* (2013), ID 350647
[6] Sharma, R., *et al.,* Partial Slip Flow and Heat Transfer over a Stretching Sheet in a Nanofluid, *Math. Prob. Eng., 2013* (2013), ID 724547
[7] Wang, C. Y., Free Convection on a Vertical Stretching Surface, *J. Appl. Math. Mech., 69* (1989), 11, pp. 418-420
[8] Rashidi. M. M., Erfani, E., The Modified Differential Transform Method for Investigating Nano Boundary-Layers over Stretching Surfaces, *Int. J. Numer. Meth. Heat Fluid Flow 21* (2011), 7, pp. 864-883
[9] Mabood, F., *et al.,* MHD Boundary Layer Flow and Heat Transfer of Nanofluids over a Nonlinear Stretching Sheet: A Numerical Study, *J. Magn. Magn. Mater*., *374* (2015), Jan., pp. 569-576

[10] Kandelousi, M. *S., et al.,* KKL Correlation for Simulation of Nanofluid Flow and Heat Transfer in a Permeable Channel, *Phy. Lett., A 378* (2014), 45, pp. 3331-3339
[11] Sheikholeslami, M., Ganji, D. D., Ferrohydrodynamic and Magnetohydrodynamic Effects on Ferrofluid Flow and Convective Heat Transfer, *Energy, 75* (2014), 1, pp. 400-410
[12] Sheikholeslami, M.*, et al.,* Ferrofluid Flow and Heat Transfer in a Semi Annulus Enclosure in the Presence of Magnetic Source Considering Thermal Radiation*, J. Taiwan Inst. Chem. Eng., 47* (2014), Feb., pp. 6-17
[13] Sheikholeslami, M.*, et al.,* Numerical Simulation of MHD Nanofluid Flow and Heat Transfer Considering Viscous Dissipation, *Int. J. Heat Mass Transf., 79* (2014), Dec., pp. 212-222
[14] Sheikholeslami, M.*, et al.,* Lattice Boltzmann Simulation of Magnetohydrodynamic Natural Convection Heat Transfer of Al_2O_3-Water Nanofluid in a Horizontal Cylindrical Enclosure with an Inner Triangular Cylinder, *Int. J. Heat Mass Transf., 80* (2015), Jan., pp.16-25
[15] Sheikholeslami, M., Ganji, D. D., Entropy Generation of Nanofluid in Presence of Magnetic Field Using Lattice Boltzmann Method, *Phys. A: Statistical Mechanics and Its Applications, 417* (2015), Jan., pp. 273-286
[16] Sheikholeslami, M., Ganji, D. D., Nanofluid Flow and Heat Transfer Between Parallel Plates Considering Brownian Motion using DTM, *Comput. Methods Appl. Mech. Engrg., 283* (2015), Jan., pp. 651-663
[17] Nield, D. A., Kuznetsov, A. V., The Cheng-Minkowycz Problem for Natural Convective Boundary Layer Flow in a Porous Medium Saturated by a Nanofluid, *Int. J. Heat and Mass Transfer, 52* (2009), 25-26, pp. 5792-5795
[18] Kuznetsov, A. V., Nield, D. A., Natural Convective Boundary Layer Flow of a Nanofluid past a Vertical Plate, *Int. J. Therm. Sci., 49* (2010), 2, pp. 243-247
[19] Khan, W. A., Pop, I., Boundary Layer Flow of a Nanofluid past a Stretching Sheet, *Int. J. Heat and Mass Transf., 53* (2010), 11-12, pp. 2477-2483
[20] Bachok, N., *et al.,* Boundary Layer Flow of Nanofluids over a Moving Surface in a Flowing Fluid, *Int. J. Therm Sci., 49* (2010), 9, pp. 1663-1668
[21] Rana, P., Bhargava, R., Flow and Heat Transfer of a Nanofluid over a Nonlinearly Stretching Sheet: A Numerical Study, *Commun. Nonlinear Sci. and Numer. Simul., 17* (2012), 1, pp. 212-226
[22] Buongiorno, J., Convective Transport in Nanofluids, *J. Heat Transf., 128* (2006), 3, pp. 240-250
[23] Abel, M. S., *et al.,* MHD Flow and Heat Transfer with Effects of Buoyancy, Viscous and Joule Dissipation over a Nonlinear Vertical Stretching Porous Sheet with Partial Slip, *Eng., 3* (2011), 3, pp. 285-291
[24] Majumder, M., *et al.,* Nanoscale Hydrodynamics: Enhanced Flow in Carbon Nanotubes, *Nature, 438* (2005), Nov., p. 44
[25] Wang, C. Y., Flow due to a Stretching Boundary with Partial Slip-an Exact Solution of the Naviere-Stokes Equations, *Chem. Eng. Sci., 57* (2002), 17, pp. 3745-3747
[26] Sahoo, B., Do, Y., Effects of Slip on Sheet-Driven Flow and Heat Transfer of a Third Grade Fluid past a Stretching Sheet, *Int. Commun. Heat Mass Transf., 37* (2010), 8, pp. 1064-1071
[27] Noghrehabadi, A., *et al.,* Effect of Partial Slip Boundary Condition on the Flow and Heat Transfer of Nanofluids past Stretching Sheet Prescribed Constant Wall Temperature, *Int. J. Therm. Sci., 54* (2012), Apr., pp. 253-261
[28] Aly, E. H., *et al.,* Analytical and Numerical Investigations for the Flow and Heat Transfer of Nanofluids over a Stretching Sheet with Partial Slip Boundary Condition, *Appl. Math. Inf. Sci., 8* (2014), 4, pp. 1639-1645
[29] Rashidi, M. M., *et al.,* Investigation of Entropy Generation in MHD and Slip Flow over a Rotating Porous Disk with Variable Properties, *Int. J. Heat and Mass Transfer, 70* (2014), Mar., pp. 892-917
[30] Rashidi, M. M., Erfani, E., Analytical Method for Solving Steady MHD Convective and Slip Flow due to a Rotating Disk with Viscous Dissipation and Ohmic Heating, *Eng. Comput., 29* (2012), 6, pp. 562-579
[31] Liao, S. J., *Beyond Perturbation: Introduction to the Homotopy Analysis Method*, Chapman & Hall, CRC Press, Boca Raton, Fla., USA, 2003
[32] Rashidi, M. M., *et al.,* Homotopy Simulation of Nanofluid Dynamics from a Nonlinearly Stretching Isothermal Permeable Sheet with Transpiration, *Meccanica, 49* (2014), 2, pp. 469-482
[33] Rashidi, M. M., Erfani, E., A New Analytical Study of MHD Stagnation-Point Flow in Porous Media with Heat Transfer, *Comput. Fluids, 40* (2011), 1, pp. 172-178
[34] Hayat, T., Nawaz, M., Unsteady Stagnation Point Flow of Viscous Fluid Caused by an Impulsively Rotating Disk, *J. Taiwan Inst. Chem. Eng., 42* (2011), 1, pp. 41-49
[35] Sajid, M., Hayat, T., Influence of Thermal Radiation on the Boundary Layer Flow due to an Exponentially Stretching Sheet, *Int. Commun. Heat Mass Transf., 35* (2008), 3, pp. 347-356

[36] Nadeem, S., *et al.,* MHD Stagnation Flow of a Micropolar Fluid through a Porous Medium, *Meccanica, 45* (2010), 6, pp. 869-880
[37] Ziabakhsh, Z., *et al.,* Analytical Solution of the Stagnation-Point Flow in a Porous Medium by Using the Homotopy Analysis Method, *J. Taiwan Inst. Chem. Eng., 40* (2009), 1, pp. 91-97
[38] Rashidi, M. M., *et al.,* Approximate Solutions for the Burger and Regularized Long Wave Equations by Means of the Homotopy Analysis Method, *Commun. Nonlinear Sci. Numer. Simul., 14* (2009), 3, pp. 708-717
[39] Rashidi, M. M., Dinarvand, S., Purely Analytic Approximate Solutions for Steady Three-Dimensional Problem of Condensation Film on Inclined Rotating Disk by Homotopy Analysis Method, *Nonlinear Anal Real World Appl., 10* (2009), 4, pp. 2346-2356
[40] Mabood, F., Khan, W. A., Approximate Analytical Solution for Influnce of Heat Transfer on MHD Stagnation Point Flow in Porous Medium, *Comput. Fluids 100* (2014), Sep., pp. 72-78
[41] Rashidi, M. M., *et al.,* Analytic Approximate Solutions for Steady Flow over a Rotating Disk in Porous Medium with Heat Transfer by Homotopy Analysis Method, *Computer & Fluids, 54* (2012), Jan., pp.1-9

Paper submitted: April 24, 2014
Paper revised: January 31, 2015
Paper accepted: Mart 6, 2015